How electrolyte shielding influences the electrical potential in transmembrane ion channels

Peter C. Jordan,*‡ Russell J. Bacquet,‡ J. Andrew McCammon,‡§ and Phouc Tran*
*Department of Chemistry, Brandeis University, Waltham, Massachusetts 02254; ‡Department of Chemistry, University of Houston, Houston, Texas 77204; and §Department of Physiology and Molecular Biophysics, Baylor College of Medicine, Houston, Texas 77030

ABSTRACT The electrical potential due to fixed charge distributions is strongly altered in the vicinity of a membrane and notably dependent on aqueous electrolyte concentration. We present an efficient way to solve the nonlinear Poisson-Boltzmann equation applicable to general cylindrically symmetric dielectric geometries. It generalizes Gouy-Chapman theory to systems containing transmembrane channels. The method is applied to three channel systems: gramicidin, gap junction, and porin. We find that for a long, narrow channel such as gramicidin concentration variation has little influence on the electrical image barrier to ion permeation. However, electrolyte shielding reduces the image induced contribution to the energy required for multiple occupancy. In addition, the presence of electrolyte significantly affects the voltage profile due to an applied potential, substantially compressing the electric field to the immediate vicinity of the pore itself. In the large diameter channels, where bulk electrolyte may be assumed to enter the pore, the electrolyte greatly reduces the image barrier to ion permeation. At physiological ionic strengths this barrier is negligible and the channel may be readily multiply occupied. At all ionic strengths considered ($I > 0.005$ M) the image barrier saturates rapidly and is essentially constant more than one channel radius from the entrance to the pore. At lower ionic strengths ($I < 0.016$ M) there are noticeable (>20 mV) energy penalties associated with multiple occupancy.

INTRODUCTION

Long range electrostatic forces are known to significantly influence ionic transport through membrane spanning channels (for recent review see Jordan, 1987). The shape of the pore, the composition and head group structure of the phospholipid membrane, charge distributions within the pore and/or its vestibule and the composition of the electrolytes bathing the membrane all contribute to electrostatic influences on channel conductance; these depend critically on the dielectric differences between the various regions of the water-membrane-pore ensemble. As has been recognized previously, the long range dielectric forces exert only a modulating effect on ion-channel interaction within the constricted region of a pore; here the dominating influence is direct coupling between an ion and nearby charged and polar groups. In the vestibules and the surrounding electrolyte, the long range interactions strongly influence ionic motion, especially the access process.

Calculations devoted to elucidating the effect that dielectric differences have on channel conductance have, with few exceptions (Levitt, 1985, 1986; Dani, 1986), not simultaneously treated the influence of varying electrolyte concentration. While it is known qualitatively that increasing ionic strength must shield the electrical potential due to any individual source (including the image forces), no accurate measure of the quantitative significance of this effect in the vicinity of an ion channel has been given. This paper, of which a preliminary account has already appeared (Jordan, et al., 1988), is devoted to rectifying this omission and describes how the coupled influence of dielectric geometry and ionic strength may affect the permeability of ion channels.

Following approaches outlined previously (Warwicker and Watson, 1982; Klapper et al., 1986), we have developed an efficient way to solve the nonlinear Poisson-Boltzmann (NLPB) equation applicable to general cylindrically symmetric dielectric geometries. In essence this approach generalizes Gouy-Chapman theory to systems containing transmembrane channels. The choice of such a restricted geometry is governed by two reinforcing considerations: detailed channel shapes are not available, consequently cylinders, even though they can not possibly precisely describe a pore, are plausible models; restrictions to cylindrical geometry reduces computational demand ≈100-fold.

We apply the technique to a particular model geometry, a right circular cylindrical pore spanning a membrane slab and investigate the effect that electrolytic shielding has on the image potential and the polarization energy due to single and multiple ion occupancy and on the voltage profile due to an applied potential. We first outline the method. Then we apply it to some geometries of special interest, in particular to narrow pores using a gramicidinlike model geometry and to wide pores using gap junction and porin as examples. Our main emphasis is on the NLPB equation because, at higher ionic strengths

0006-3495/89/06/1041/12 $2.00

(≥0.1 M), there are notable effects due to nonlinearity. These manifest themselves in differences caused by changes in electrolyte valence (at constant ionic strength) and to a breakdown of superposition when channels are multiply occupied.

THEORY

Our geometrical model of an ion pore is illustrated in Fig. 1. Here the electrical source is an ion located on the axis of the pore. The aqueous regions, of dielectric constant 80, contain identical electrolytes. The membrane dielectric constant is 2 and that of the aqueous pore is variable. When the pore is large (e.g., porin or gap junction), ϵ would be 80. When it is narrow (e.g., gramicidin or K-channel), ϵ is not known. The membrane width is W and the pore's electrical radius (a quantity somewhat larger than its physical radius: Jordan, 1981, 1984*a*; Levitt and Decker, 1988) is a_o. In the equilibrium electrolyte (the regions to the right of $z = L$ and the left of $z = -L$ and, in the case of a nonselective channel, the channel itself), the Poisson-Boltzmann equation applies

$$\nabla \cdot [\epsilon(r)\nabla\phi(r)] + 4\pi\rho_B(r) + 4\pi p_o(r) = 0 \qquad (1a)$$

$$\rho_B(r) \equiv \sum_{\alpha=1}^{\nu} N_\alpha(r) z_\alpha e_o = \sum_{\alpha=1}^{\nu} N_\alpha z_\alpha e_o \exp\left[-z_\alpha e_o \phi(r)/k_B T\right], \qquad (1b)$$

where $\epsilon(r)$ is the local dielectric constant, $\phi(r)$ the local potential, $\rho_B(r)$the smeared out background charge density arising from charge separation in the electrolyte, $\rho_o(r)$ the charge density due to the source, $N_\alpha(r)$ the local number density of ions of type α (N_α are the bulk, equilibrium values), z_α their valence, e_o the electronic charge, k_B Boltzmann's constant, and T the temperature. The identity in Eq. 1b simply relates charge density to ionic concentration; the equality, incorporating the Boltzmann factor, presumes local equilibrium. We assume that bulk electrolyte is excluded from the membrane and, if the channel is either ion specific or valence selective, from the pore as well. We account for ionic size by assuming further that electrolyte is excluded from regions within one ionic radius of an ionic source. Thus, in the regions from $z = -L$ to $z = L$, Eq. 1 reduces to Poisson's equation when $s \geq a_o$ in all instances and, for selective pores, for all s,

$$\nabla \cdot [\epsilon(r)\nabla\phi(r)] + 4\pi\rho_o(r) = 0. \qquad (2)$$

Eq. 2 is simply the full Poisson-Boltzmann equation in the absence of back-ground charge density. If the electric potential $\phi(r)$ is small enough, Eq. 1 can be linearized and it simplifies to the familiar Debye-Hückel equation.

Rather than trying to find an analytical solution to the underlying differential equation, it is computationally more practicable to reformulate the problem so as to generate a finite-difference solution in a way that explicitly utilizes the constraint of cylindrical symmetry. By analogy to the approach outlined by Klapper et al. (1986) the various functions $\phi(r)$, $\rho(r)$, and $\epsilon(r)$ are approximated at points (k, n) on a regular cylindrical grid of mesh size Δs in the radial direction and Δz in the axial direction. $\phi(r)$ is thus to be determined on a set of rings, $s = k\,\Delta\,s$, $0 \leq k \leq \infty$, and $z = n\,\Delta\,z$, $-\infty \leq n \leq \infty$. Because of the constraint of cylindrical symmetry, these are equipotentials. The potential on a representative ring is determined by averaging $\phi(r)$ over those regions which lie closer to the specified ring than to any other ring; it is thus determined by the integral $\int\int\phi(r)dzsds\theta$.

Unlike normal box integration (Scarborough, 1962), all cells are not equivalent. The axial cell must be handled slightly differently from any annular cell because the annular index k only ranges from 0 to ∞; there are no annuli with $k < 0$. Typical axial and annular cells are illustrated in Fig. 2 which highlights the distinction between the integration grid and the grid points for evaluationg ϕ. It is crucial to locate the cell boundaries halfway between the grid points at which ϕ is evaluated because in our finite difference approach the constraint that the normal component of the electric displacement vector is continuous at electrical phase boundaries is used repeatedly; this condition is most easily treated with the integration cells defined in this way. Thus z-integration is between $(n - \frac{1}{2})\Delta z$ and $(n + \frac{1}{2})\Delta z$.

For an axial cell s-integration is between 0 and $\frac{1}{2}\,\Delta\,s$; for annular cells it is between $(k - \frac{1}{2})\Delta s$ and $(k + \frac{1}{2})\Delta s$. Integrating Eq. 1a over the volume of a cell of Fig. 2

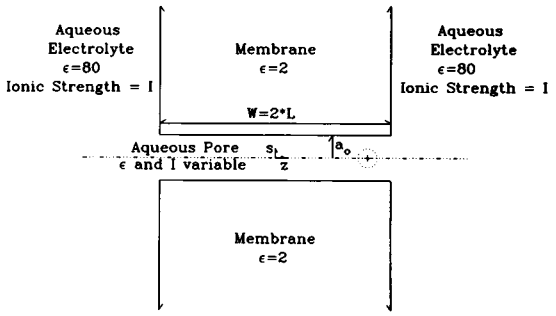

FIGURE 1 Geometry of the cylindrically symmetric membrane-electrolyte system. There are three well articulated domains. The regions to the right and left of the membrane contain aqueous electrolyte. A sharp boundary between electrolyte and pore is assumed. In the pore ($s > a_o$, $-L < z < L$), both ϵ and I may be adjusted to suit the physiological model of interest. To conform to the restriction of cylindrical symmetry the ion is always located axially. The coordinate s measures radial distance in the x-y plane, $s = \sqrt{(x^2 + y^2)}$.

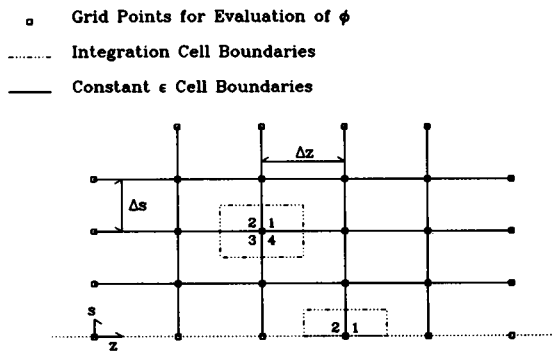

FIGURE 2 Projection of integration and dielectric grid. The system has cylindrical symmetry. Each integration annulus surrounds the equipotential rings on which ϕ is evaluated. The grid spacings, Δz and Δs, need not be equal. The axial integration cells are qualitatively distinct from all others. The quadrants surrounding the grid point in the two integration cells are denoted.

yields

$$\iiint \nabla \cdot [\epsilon(r)\nabla\phi(r)]dzsdsd\theta + \iiint 4\pi\rho_B(r)dzsdsd\theta + \iiint 4\pi\rho_o(r)dzsdsd\theta = 0. \quad (3)$$

Evaluation of Eq. 3 is slightly different for axial and nonaxial cells. For an axial cell, the second integral is $\sim(\pi\Delta s)^2\Delta z\rho_B(0, n)$ where $\rho_B(0, n)$ is calculated from Eq. 1b. The background charge density is determined by the average local potential $\phi(0, n)$ and the ionic concentrations N_α in the regions surrounding the point $(0, n)$. The third integral is $4\pi q_o$, where q_o is the total fixed charge inside the volume element. The first term is transformed to a surface integral using Gauss's theorem; the result is

$$\iint \epsilon(r)\nabla\phi(0, n) \cdot dA + (\pi\Delta s)^2\Delta z\rho_B(0, n) + 4\pi q_o = 0. \quad (4a)$$

A finite difference approximation to the gradient operator in the first term yields, after integration over the axial cell,

$$\pi(\Delta s)^2/\Delta z\{\epsilon_+[\phi(0, n + 1) - \phi(0, n)] + \epsilon_-[\phi(0, n - 1) - \phi(0, n)]\} + \pi\Delta z\epsilon_o[\phi(1, n) - \phi(0, n)], \quad (4b)$$

where the various ϵ's are defined by properly weighted averages on the surfaces of integration. It is in evaluating the surface integrals that we rely on the continuity of the normal component of the electric displacement vector. Along a ring, the analogues to Eq. 4, a and b are

$$\iint \epsilon(r)\nabla\phi(k, n) \cdot dA + 8k(\pi\Delta s)^2\Delta z\rho_B(k, n) + 4\pi q_o = 0 \quad (5a)$$

$$\pi(\Delta s)^2/\Delta z\{\epsilon_+[\phi(k, n + 1) - \phi(k, n)] + \epsilon_-[\phi(k, n - 1)] - \phi(k, n)]\} + \pi\Delta z\{\epsilon_l[\phi(k - 1, n) - \phi(k, n)] + \epsilon_o[\phi(k + 1, n) - \phi(k, n)]\}. \quad (5b)$$

In Eqs. 4 and 5, ϵ_+ is averaged on the circular face at $(n + \frac{1}{2})\Delta z$, ϵ_- averaged on the face at $(n - \frac{1}{2})\Delta z$, ϵ_o averaged on the cylindrical shell at $(k + \frac{1}{2})\Delta s$ and ϵ_l averaged on the shell at $(k - \frac{1}{2})\Delta s$. Explicit expressions for the various ϵ's appearing in Eqs. 4 and 5 are

$$\epsilon_+ = (k + \tfrac{1}{4})\epsilon_1 + (k - \tfrac{1}{4})\epsilon_4 \quad \epsilon_- = (k + \tfrac{1}{4})\epsilon_2 + (k - \tfrac{1}{4})\epsilon_3$$
$$\epsilon_o = (k + \tfrac{1}{2})[\epsilon_1 + \epsilon_2] \; [\epsilon_1 = (k - \tfrac{1}{2})\epsilon_3 + \epsilon_4], \quad (6)$$

where the ϵ_i are the dielectric constants in the cell containing the ith quadrant surrounding a field point (k, n) as illustrated in Fig. 2.

Eqs. 4, 5, 6, and 1b completely establish $\phi(k, n)$ for any given electrical source. The system is truncated in both axial and radial directions. Rather than setting the potential to zero at the boundaries, we assume a constant field in the normal direction. With these provisos, the equations can be solved iteratively; however, underrelaxation is usually necessary to avoid undamped oscillations. To accurately establish the potential requires iterating until the mean square change in successive iterations is $\leq 10^{-5}$; in some cases (particularly at low ionic strength) convergence is not obtained until the deviation is $\leq 10^{-6}$.

Because we have limited consideration to cylindrically symmetric systems, the computations can be carried out rapidly and we can calculate the potential due to an ion located at arbitrary axial positions. For a gramicidinlike geometry with W = 25 Å and a_o = 2.5 Å, we normally used a radial grid spacing of 0.625 Å and an axial spacing of 1.25 Å. With this grid, ~50 radial points and 75 axial points were adequate to obtain an accurate approximation to the electrical potential in a gramicidinlike channel.

There is one final practical consideration. To exclude electrolyte from regions close to the ion, we define $N_\alpha(r) = 0$ in cells within one ionic radius of any particular discrete charge source.

The quantities which appear in the calculations are cell averages. This means that the point electrical sources have also been approximated by smeared out cell average charge densities. Consequently the potentials we calculate are not identical to the solutions for point sources. However, as long as the focus is on cells that do not neighbor the cell containing the source, the results are invariant to further decrease cell size. For this gramicidinlike case, with z-spacings of 1.25 Å, accurate results are obtained in axial cells at least 2.5 Å from the source.

The cell averaging process does not limit our ability to compute the polarization energy of the ion. At any point the total electrical potential can be viewed as dependent on three contributions: coulombic, polarization, and electrophoretic. The coulombic term is the potential in a uniform system (constant ϵ and I). The electrophoretic term is the change in the potential due to electrolyte exclusion from the various regions (the membrane and, in the case of selective pores, the channel). The polarization

term is the change in the potential due to the dielectric differences in the system. Defined in this fashion, each term can be calculated separately. The electrophoretic energy can be exactly computed by means of a difference calculation in which the ion is located at the position of interest (ϵ is 80 everywhere, and the ionic strength in the membrane (and, for narrow channels, the pore) domain is changed from I to 0. Similarly, the polarization energy can be exactly computed by means of a subsequent difference calculation in which the ion remains at the same position, the ionic strengths are unaltered, and the dielectric constants of the membrane (and pore) domains are changed from 80 to the values of interest. The potential change at the location of the ion yields, in the first instance, the electrophoretic energy, and in the second, the polarization energy. The total image energy is the sum of the electrophoretic and polarization contributions. Both electrophoretic and polarization energies, defined in this fashion, are totally independent of cell size.[1]

By suitably modifying Eq. 1, the same general approach can be used to compute the voltage profile due to an applied potential. There is no longer an inhomogeneous source so $\rho_o(r)$ is zero. However, the reference potential is different on both sides of the membrane; to incorporate this condition, Eq. 1b must be slightly modified. As long as electrolyte is excluded from the pore, the Boltzmann relationship can be applied separately on either side of the membrane and the smeared out charge density due to charge separation in the electrolyte is, on the left hand side of the membrane, given by

$$\rho_L(r) = \sum_{\alpha=1}^{r} N_\alpha z_\alpha e_o \exp\left[-z_\alpha e_o\{\phi(r) - V_L\}/k_B T\right], \quad (7)$$

where V_L is the reference potential to the left of the membrane; on the right hand side ρ_L is replaced by ρ_R and V_L by V_R. As written, charge separation arises because this local potential differs from the relevant electrode potential. This formulation is valid if diffusion through the channel is rate limiting, i.e., if the pore is sufficiently narrow and the concentration of permeant ion sufficiently high. More generally local equilibrium does not apply and the ionic concentrations are not simply given by a Boltzmann distribution established by $(\phi[r] - V)$; they also may depend upon the current. In the latter case Eq. 7 must be replaced by

$$\rho_B(r) = \sum_{\alpha=1}^{r} z_\alpha e_o N_\alpha(r) \quad (8)$$

and, if the system is in a steady state, the full Nernst-Planck equation should be solved in order to relate potential and concentration; this greatly complicates the analysis (see e.g., Levitt, 1985, 1986; Peskoff and Bers, 1988). However, as long as this is unnecessary, Eq. 7 can be substituted for Eq. 1b and the iterative method used to solve for the potential profile. Convergence is less readily attained; the mean square change between successive iterations must be $\leq 5 \cdot 10^{-8}$. The reason for this is readily apparent. Here we are interested in the relatively small deviations of the potential profile from the limiting case, a uniform membrane slab where the electric field only deviates from zero within the membrane. Far from the pore, the potential profile differs little if any from that in a channel free membrane. Thus, at most locations the limiting profile is an excellent approximation to the exact result.

[1]We are indebted to Professor Barry Honig for pointing this out.

RESULTS AND DISCUSSION

General features

Unlike the simpler case of dielectric shielding in the absence of electrolyte, the electrical properties of the system can not be scaled in terms of a single parameter. Nonetheless, Eq. 1 does permit some parameterization. The axial image potential (or voltage profile, in the case of an applied potential), $\phi(z; z_o)$, where z_o is the location of the permeant ion (for the case of the image problem), can be written in terms of reduced variables

$$\phi(z; z_o) = (e_o/a_o\epsilon_1) \cdot F(\zeta; \zeta_o, L/a_o, \epsilon_2/\epsilon_1, \lambda_D/a_o, \{z_\alpha\}), \quad (9)$$

where λ_D is the Debye length and ζ is z/a_o, etc. When the Poisson-Boltzmann equation can be linearized, the results depend only on ionic strength through λ_D and not specifically on the valence of the electrolyte. The significance of the relationship expressed by Eq. 9 is that the potential profile for a given pore geometry and ionic strength is identical in shape to that for a pore with the same geometry at a scaled ionic strength. For example, the potential profiles are identical if a_o is increased by a factor of 1.21 while ionic strength is decreased by a factor of 1.1.

Model calculations for a narrow, gramicidinlike pore

Fig. 3 *a–c* illustrate the effect that changing ionic strength in 1-1 electrolytes has on the electrical potential due to an ion located at representative axial positions in a gramicidinlike pore, assuming the geometry of Fig. 1 and that ϵ within the pore is 80. The pore (and membrane) is 25 Å long; its electrical radius is chosen to be 2.5 Å. In order to account for the influence of the polar moieties lining the interior of the pore, this is somewhat greater

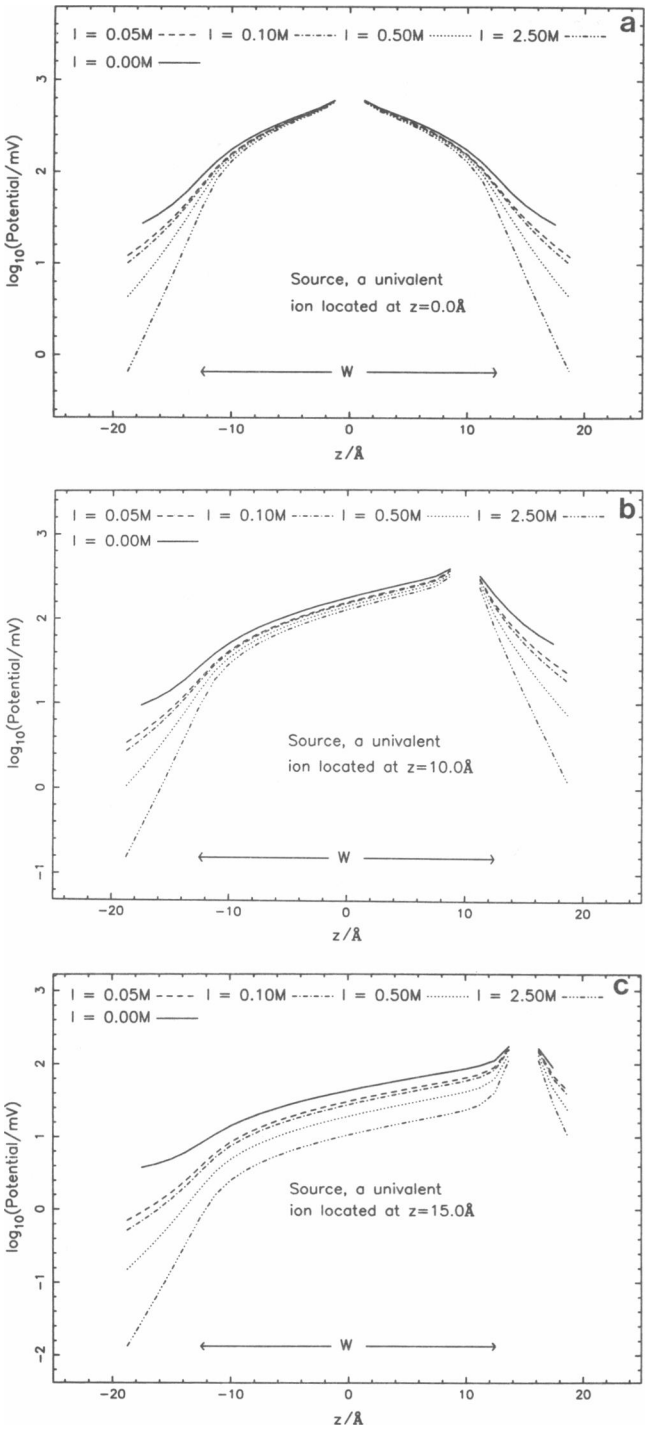

FIGURE 3 Electrical potential in a gramicidinlike pore for a model where ϵ_{pore} is 80 and electrolyte is excluded from the pore. The pore is 25 Å long with an electrical radius of 2.5 Å. The ionic strength varies from 0.0 to 2.5 M. Outside the pore the potential attenuates essentially exponentially. The region in the immediate vicinity of the ionic source (where the numerical solution is unreliable and the potential diverges) is excluded. Three cases are contrasted, a source located at $z = 0$ Å, $z = 10$ Å, and $z = 15$ Å.

than the physical radius of the lumen, ≈2.1 Å (Jordan, 1981, 1984*a*; Levitt and Decker, 1988). As already pointed out, for the ionic strengths considered (0.01 to 2.5 M), results independent of system size are obtained with a radial cutoff of 31.25 Å and an axial cutoff of ±95 Å. In general, results are independent of grid size at separations two or more grid spacings from the location of the source. Improved estimates of the potential near the ion can be given by using a finer grid size. For the model gramicidin studies radial and axial spacings of 0.625 and 1.25 Å respectively, were used; here, this spacing yields accurate values of ϕ at distances as close as 2.5 Å to the ion, a separation far less than any realistic interionic separation in a multiply occupied channel. An ionic radius of 1.0 Å was assumed.

The qualitative behavior of the electrical potential is precisely that expected. Increasing electrolyte concentration shields the potential. Exterior to the pore and sufficiently far from the membrane the potential falls off exponentially, consistent with Gouy-Chapman theory. Within the pore (at least 2 a_0 from the pore mouth) there are only small relative changes in the potential, rarely more than 15%, even when ionic strength changes drastically, from nonelectrolyte to 2.5 M concentration.

However, the actual changes in electrical potential can be significant, thus affecting the pore's ability to solvate a second cation. With an ion located near one mouth of the pore, e.g., at +10 Å, the potential at the corresponding site near the other mouth, −10 Å, decreases by 30 mV as ionic strength is increased from 0.0 to 2.5 M. With the ion still located at +10 Å, the same change in ionic strength reduces the potential at the channel center by more than 50 mV. Consequently shielding could substantially increase the ability of a pore to solvate a second ion and reduce the barrier to ion translocation when a second ion enters the channel. The influence of ionic strength of the access process for a second ion is dramatically clear from Fig. 3 *b* and *c*. Here one ion is located in the mouth, at +10 Å or in bulk, at +15 Å. In going from 0.0 to 2.5 M the electrical potential at the complementary site drops by 70 mV. Again, shielding greatly promotes second ion accessibility.

Not only does electrolyte shielding have a substantial influence on the electrical potential due to an ionic source in the channel, there are also significant differences due to electrolyte valence. A 3-3 electrolyte reduces the electrical potential substantially more than a 1-1 electrolyte, even at the same ionic strength, suggesting that monovalent cation multiple occupancy would be enhanced by using polyvalent electrolytes as the aqueous media (assuming that competitive blocking did not interfere). This is shown in Fig. 4 *a–d* for ions located at $z = 0$ Å and 10 Å. For an ion located at +10 Å, consider the changes at +15 Å. At 0.1 M ionic strength, the valence

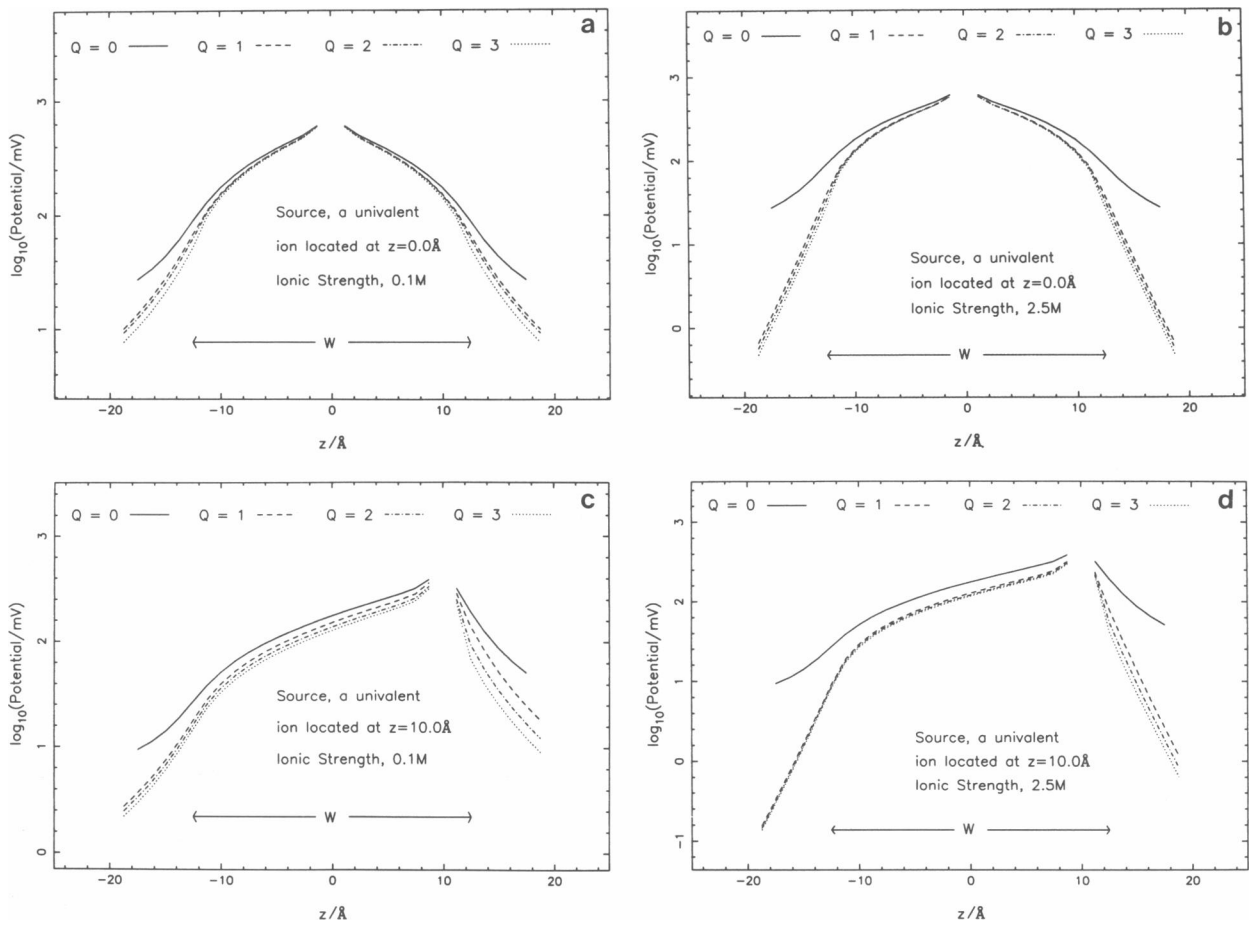

FIGURE 4 Effect of electrolyte valence (here denoted as Q) on the electrical potential in a gramicidinlike pore; for comparison, the potential at zero ionic strength ($Q = 0$) is also shown. The model is that of Fig. 3. Four cases are contrasted in order to illustrate the effect of ionic strength and ion location, $I = 0.1$ M, $z = 0$ Å; $I = 2.5$ M, $z = 0$ Å; $I = 0.1$ M, $z = 10$ Å; and I 2.5 M, $z = 10$ Å. At high ionic strength changing electrolyte valence has relatively less influence on the electrical potential. Outside the pore the potential again attenuates exponentially. The region in the immediate vicinity of the ionic source is again excluded.

change reduces the potential by another 25 mV. At 2.5 M, the effect is much smaller, only 10 mV, probably because shielding at such high ionic strengths was almost complete in the 1-1 system. The effect of valence should also be notable at locations within the channel. With the ion still at +10 Å, at 0.1 M, changing from 1-1 to 3-3 electrolyte lowers the potential at the channel midpoint by 30 mV; at 2.5 M, the effect is again smaller, ≤10 mV. If the ion is located at the channel midpoint, a similar qualitative picture is again evident.

As already noted, shielding sharply reduces electrostatic repulsion in a doubly occupied channel. In addition, there is a small cooperative effect. With one monovalent ion located at +10 Å, the image contribution to the interionic repulsion potential at the symmetrical −10 Å location is less than would be expected simply on the basis of superposition. As double occupancy calculations are quite computer intensive, we have only treated a few cases. With ions located at ±10 Å, and for ionic strengths between 0.1 and 1.0 M, the repulsion potentials are reduced a further 6 mV. This is a manifestation of the nonlinearity of the problem; the solutions to the linear Poisson-Boltzmann (LPB) equation are strictly superposable.

A separate measure of the limitations of an LPB calculation is given by direct comparisons of the solutions to the linear and nonlinear equations. At low ionic strength, $I \leq 0.05$ M, there are no important differences unless the ion is located within the channel and close to its mouth; in this case the calculated potentials differ by 5 to 15 mV in the region from 2.5 to 5 Å from the ion; the solution to the LPB is always numerically the larger.

When I increases to 0.5 M noticeable differences are found unless the ion is located well within the pore. For an

ion within 5 Å, ≈ one Debye length, of the mouth, potential differences of as much as 30 mV are found in the region from 2.5 to 5 Å from the source.

As described previously, a difference calculation can be used to exactly compute the polarization energy (the energy required to polarize the membrane, excluding the electrophoretic effect). The results are shown in Fig. 5 for the gramicidinlike test case. Increasing ionic strength in 1-1 electrolyte reduces the polarization energy. However, the only significant effects (energy shifts ≥ thermal energy, 2.5 kJ mol^{-1}) are inside the channel, near the channel mouth (this is most clearly illustrated in Fig. 6). Here the polarization energy is still sizable and the ion is in close proximity to the electrolyte. For an ion at the +10 Å location, the polarization energy drops by 2.5 kJ mol^{-1} as ionic strength increases to 2.5 M. The shape of the five curves illustrated is remarkably similar. In fact, accurate estimates of the effect of ionic strength on the potential at an arbitrary location in the channel can be obtained from the 0.0 M polarization potential and the effect of ionic strength variation on the peak in the polarization energy. The basic observation is that all five curves are nearly parallel. As a result, we find the approximate relationship

$$E(z - a_0 K \delta E_0 s/c; I) \approx E(z; 0) - \delta E_0/c$$
$$s = K dE(z; 0)/dz, \quad c = \sqrt{[1 + s^2]},$$
$$K = a_0 \epsilon_1 / e_0^2,$$
$$\delta E_0 = E(0; 0) - E(0; I). \qquad (10)$$

The influence of varying ionic strength for ionic sources at selected locations is illustrated in Fig. 6. At low values of I, the displacements are essentially proportional to $\sqrt{I}$, typical of ionic strength effects generally. The small deviations from linearity noted in the extrapolation to zero ionic strength provide an indication of the numerical uncertainties in the calculation. Most of the I-variation occurs for $I \leq 0.25$ M; further increasing I has notably less influence on the polarization energy. The slopes of the curves for ions located at 0, 5, and 15 Å are nearly parallel.

The electrophoretic effect accounts for the energy needed to remove an ion from the aqueous electrolyte and place it in an electrolyte-free region with the same dielectric properties. This is an endothermic process and thus increases the energy barrier so that the total electrostatic contribution to the energy of an ion in the model pore is little different from its value in the electrolyte-free system. In fact, as illustrated in Fig. 7, the electrophoretic influence, near the center of the pore, overcompensates for the electrostatic shielding. The net effect, in this domain, is that the electrostatic energy increases with increasing ionic strength. There is an isosbestic point near

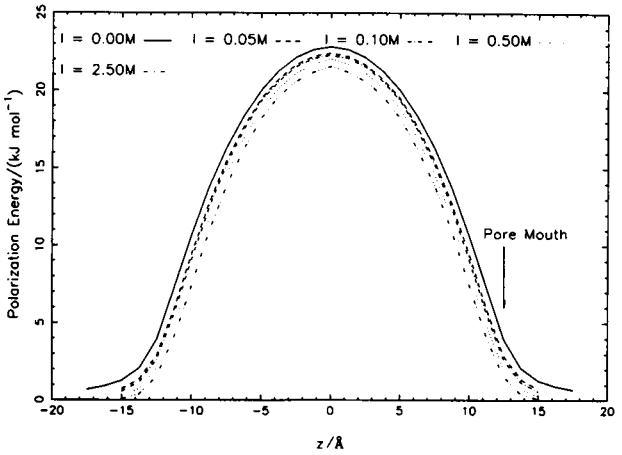

FIGURE 5 Plot of polarization energy (defined as the energy change in altering the dielectric constant in the membrane domain from 80 to 2, see text), as a function of ion position in a gramicidinlike pore. Ionic strengths in the range 0.0 to 2.5 M are compared. For this long narrow pore varying electrolyte concentration has little influence on the polarization energy.

the 5 Å location. Further from the center of the pore electrolyte shielding dominates and the energy barrier behaves as expected, decreasing with increasing ionic strength. Fig 8 illustrates the concentration dependence of the electrophoretic contribution to the total energy shift. Not surprisingly, it is never very large, is negligible outside the pore, increases rapidly as the ion enters the pore, increases rapidly with increasing ionic strength, and is essentially proportional to $\sqrt{I}$; it also appears to saturate in the vicinity of 5 Å from the pore midpoint. The

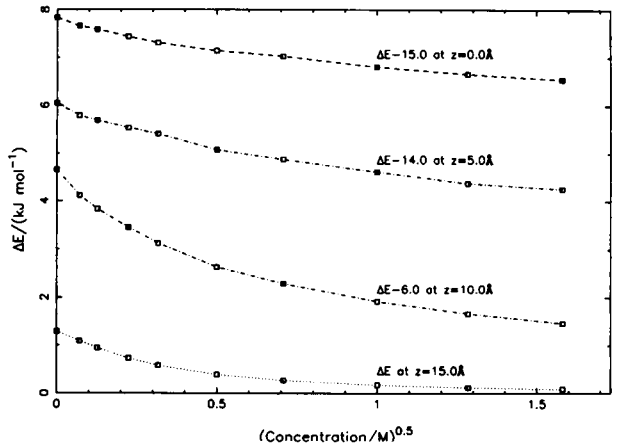

FIGURE 6 Effect of ionic strength on the polarization energy (ΔE) at selected locations in the gramicidinlike model pore. For ease of comparison, the energy plots have been displaced. At low ionic strength the plots become essentially linear in $\sqrt{I}$.

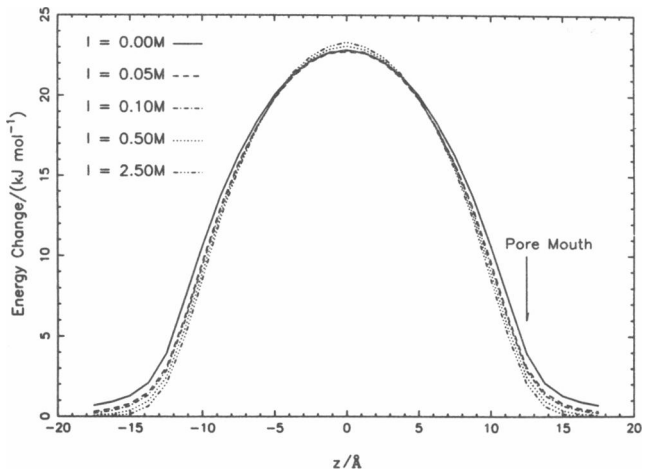

FIGURE 7 Plot of total image energy (defined as the energy change in bringing the ion from bulk electrolyte to a specific location in the pore with no change of ϵ in the medium immediately surrounding the ion, see text), as a function of ion position in a gramicidinlike pore. Ionic strengths in the range 0.0 to 2.5 M are compared. Surprisingly, the image energy increases as ionic strength increases for regions in the center of the channel, reflecting the electrophoretic contribution. Closer to the pore mouth electrolyte shielding lowers the image energy.

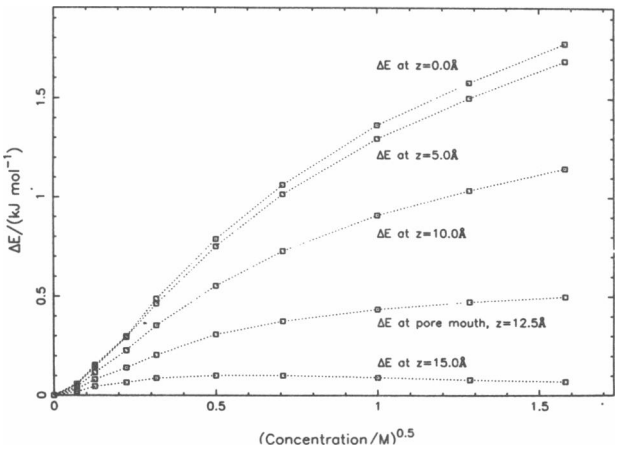

FIGURE 8 Effect of ionic strength on the electrophoretic energy (ΔE, see text) at selected locations in the gramicidinlike model pore. At low ionic strength the plots become essentially linear $\sqrt{I}$. That the curves do not precisely extrapolate to zero provides a measure of the computational error.

fact that the curves do not extrapolate cleanly to the origin is again an indication of the extent of computational inaccuracy introduced by the finite grid approximation.

Fig. 9 summarizes the results of our calculations of voltage profiles due to an applied potential difference, V_o.[2] Some numerical calculations were carried out at ionic strengths as low as 0.001 M; in this case many more grid points were needed in order to obtain adequate convergence. Here, the maximum values of both s and z had to be more than 200 Å (the Debye length is 97 Å). To a high degree of approximation, the voltage profiles can be scaled in terms of V_o. However, for a total voltage drop of 500 mV ~50 mV of the drop occurs in each of the bulk electrolytes; at the highest ionic strength considered (10.0 M), this reduces to 25 mV. There are essentially insignificant differences in the shape of the potential profiles as V_o increases; for I's from 0.1 to 10.0 M and an applied potential of 500 mV the exact potential drop in bulk electrolyte is ≈0.3 mV less than the value determined by scaling. Only if V_o could be increased to the unattainable value of 3,000 mV would there be significant deviations; the exact result would then be ≈15–45 mV less than the scaled value, depending upon ionic strength. It is evident that, within the channel, the constant field approximation is well satisfied (due to the pore's constant radius) and that shielding saturates rapidly as ionic strength

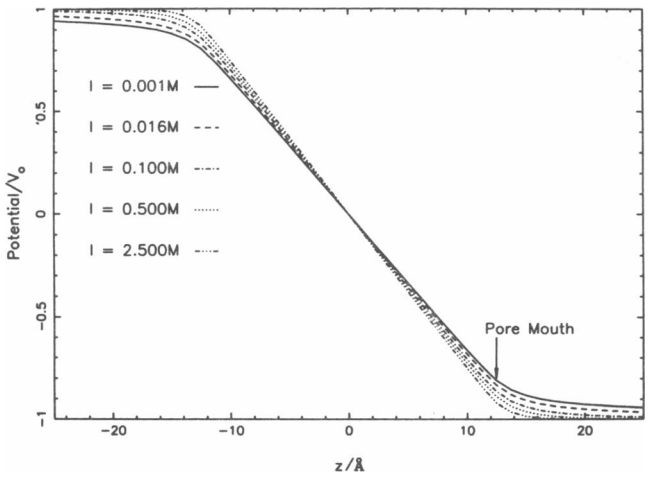

FIGURE 9 Voltage profiles as function of ionic strength in the gramicidinlike pore. As the pore is of constant radius, within the channel the constant field approximation is reliable. No comparison with an I = 0.0 M plot is possible because the calculations presented previously (Jordan, 1982, 1984*b*) describe a different model (see footnote 2).

[2]Extrapolation to zero ionic strength does not limit to the approximate values presented in our earlier studies (Jordan, 1982, 1984*b*). In that work we assumed that the electrical potential profile due to an applied voltage difference is identical to the profile arising when properly chosen uniform charge densities are placed at the membrane-water interfaces. This procedure is equivalent to assuming that the electric field discontinuity at the membrane-water interface is constant everywhere along that boundary, an approximation that is strictly correct only in the limit of very long, narrow pores (Levitt, 1978). In fact, that approximation overestimates the electric field discontinuity, and consequently overestimates the field in the region $-L < z < L$ and underestimates it in the aqueous regions.

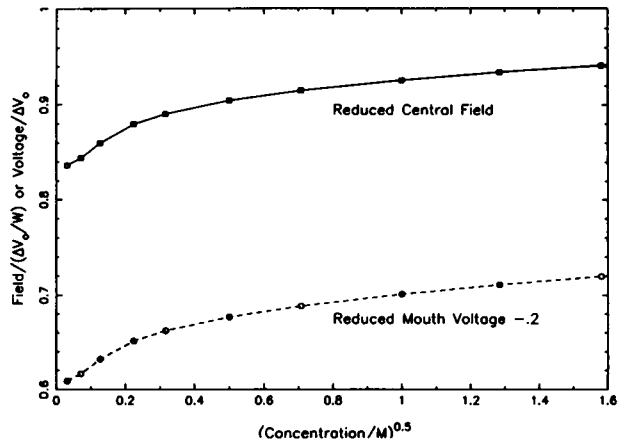

FIGURE 10 Effect of ionic strength on the central field and on the voltage at the pore mouth for the gramicidinlike model. For ease of comparison, the plot of mouth voltage has been displaced. At low ionic strengths the behavior is essentially linear in $\sqrt{I}$. As noted in Fig. 9, exact calculations in the limit that $I \rightarrow 0.0$ M are not available.

increases. There is a noticeable effect of ionic strength on the electrical distance at the binding site ≈1.25 Å inside the channel mouth (≈11.25 Å from the midpoint). At the highest I illustrated, 2.5 M, the voltage drop at this site is ~12.5%; when I is 0.1 M, the drop is 14.7%; at 0.001 M it is 16.9%. While these percentage changes are small, they might translate into respectable voltage differences, at least at high applied potentials. For a total drop of 500 mV, the change in voltage drop to this site in going from 0.001 M to 2.5 M would be 22 mV, enough to effect the kinetics of ion transport.

As was the case for both the polarization and electrophoretic energies, both the electric field at the channel midpoint and the voltage drop at the channel mouth exhibit a $\sqrt{I}$ dependence at low ionic strength. The two curves are essentially parallel as shown in Fig. 10.

Realistic model for gramicidin

The value of ϵ used to describe the properties of the channel water is quite arbitrary. Because pore water is about half as dense as bulk water, an equally plausible value for ϵ would be 40. Molecular dynamics calculations, using a polarizable water model (P. C. Jordan, manuscript submitted for publication), indicate that the mean dipole moment of channel water is substantially less than that of bulk water (2.3 D rather than 2.45 D), also arguing for a smaller ϵ. For purposes of comparison, the electrical geometry is presumed to be the same as that used when $\epsilon = 80$.[3] Table 1 illustrates the effect of reducing ϵ on a number of quantities of interest. The potential change that occurs when the ion is removed from the aqueous electrolyte to a point within the pore is now composed of three contributions: the change in ionic self energy due to solvation in a region of lower dielectric constant, the polarization energy, and the electrophoretic energy. To separate the self energy term we imagine surrounding the whole electrical ensemble with extra slabs of electrolyte of the same ionic strength but with $\epsilon = 40$. For an ion in the channel, the total image (polarization plus electrophoretic) term is calculated assuming a reference state with $\epsilon = 40$; of course, the region immediately outside the pore still has $\epsilon = 80$. For an ion in the electrolyte the reference state is one with an $\epsilon = 80$. Well within the pore the image energy is increased by a factor of ≈1.5 due to the lowering of the dielectric constant. Nearer the pore mouth and in the bulk solution the decrease in dielectric constant has little effect on the image energy. At both locations considered, electrophoretic effects are prominent. The image energy increases with increasing ionic strength, due to the sizeable energy required to remove an ion from electrolyte.

Because the pore interior is not as permittive, the voltage drop in this system is much more nearly confined to the pore itself. In 0.1 M electrolyte, ≈92% of the voltage drop is confined to the pore when ϵ is reduced to 40; for an ϵ of 80, only 86% was. Similarly the field at the

[3]In fact, the electrical radius of the pore should be somewhat larger because the dielectric difference between the solvent in the pore interior and the polar groups lining the channel is somewhat reduced. Using the approach outlined previously (Jordan, 1981), a better estimate of a_0 would be ≈ 2.6 Å. For computational simplicity, the value of 2.5 Å is retained.

TABLE 1 Comparison of selected properties of a realistic gramicidinlike pore ($\epsilon_{pore} = 40$) with test case ($\epsilon_{pore} = 80$) as a function of ionic strength

	Total image energy/($kJ\ mol^{-1}$)							
	$z = 0.0$ Å		$z = 10.0$ Å		Central field/(V_0/W)		Mouth potential/(V_0)	
I/M	$\epsilon = 80$	$\epsilon = 40$	$\epsilon = 80$	$\epsilon = 40$	$\epsilon = 80$	$\epsilon = 40$	$\epsilon = 80$	$\epsilon = 40$
0.1	22.8	35.2	9.5	13.2	0.892	0.940	0.863	0.917
0.5	23.1	36.2	9.0	13.4	0.915	0.956	0.888	0.935
1.0	23.2	36.6	8.8	13.5	0.926	0.963	0.901	0.945
2.5	23.3	37.0	8.6	13.6	0.941	0.972	0.920	0.955

pore center is substantially increased; when the dielectric constant is smaller it is 94% of the field within the membrane while for the higher dielectric it is only 89%. Again, as the model pore is of constant radius, the constant field approximation is well satisfied in the pore interior.

Large pores

Electrolyte has a much greater influence on the electrical potential and the image energy for large diameter pores such as the gap junction and porin than it does for a pore like gramicidin. While gap junction is not a uniform cylinder (Makowski et al., 1984), reasonable geometrical parameters in a cylindrical approximation are $W = 150$ Å (Unwin and Zampighi, 1980) and $a_0 \approx 8$ Å (Flagg-Newton et al., 1979; Weigandt et al., 1982). Consequently we assume that electrolyte can enter the pore and maintain roughly the same concentration as in the bulk solutions. The effect of shielding on the image energy for an ion on the pore axis is dramatic, as illustrated in Table 2. At 0.1 M, the maximum image energy is less than 0.25 kT so that the surrounding dielectric would have almost no influence on conductance. Even at the lowest ionic strength investigated, 0.005 M, the peak in the image energy is only ≈1.2 kT, which would reduce conductance to about one-third its value at 0.1 M. Over the concentration range considered the image energy is always far less than its value in electrolyte-free solution, ≈4 kT. The presence of electrolyte almost totally shields an axially located ion from the influence of the low dielectric domain. Over the range of ionic strengths considered, 90% of the increase in the image interactions occur within 15 Å (2 a_0) of the channel mouth (2/3 within the first 7.5 Å); further translation through the interior of the channel is not influenced by the surrounding dielectric. Naturally in such a large channel the ion need not be on the axis. However, the electrostatic influence of the surrounding low ϵ region would tend to repel the ion and favor axial trajectories (Vayl and Jordan, 1987); as an ion moved close to the wall of the channel, the image energy might increase by as much as a factor of 3 (assuming a minimum ionic radius of 1.0 Å). Polarization provides a force tending to locate the ion axially; electrolyte shielding nearly eliminates the axial image barrier.

With an ion located at a fixed axial position, planes of constant z within the pore (planes perpendicular to the channel axis) are essentially equipotentials if they are more than a distance $\approx a_0$ inside the channel mouth. Only in the immediate vicinity of the ion, in the bulk solution and near the channel mouth is there a radial component to the potential within the high ϵ regions. Furthermore, the electrolyte strongly shields the potential within the channel. Table 3 summarizes the effect that decreasing ionic strength has on the axial distance at which the electrical image potential induced by an ion in the channel falls below 20 mV and below 10 mV. At 0.1 M, the total interaction potential between a pair of ions in the channel (both direct and image induced) is below 20 mV for axial separations as small as 15 Å; at 0.005 M, an interionic axial separation of >50 Å is required for the same effect. Consequently, at physiological ionic strengths, the gap junction could accommodate a substantial charge imbalance; at very low (or zero) ionic strength, interionic repulsion is significant and multiple occupancy would be unfavorable.

TABLE 3 Effect of ionic strength on axial separation at which the image interactions between a pair of ions in the gap junction analogue channel are below 10 mV and 20 mV, respectively

I/M	Image interaction < 20 mV z/Å	Image interaction < 10 mV z/Å
0.000	100	120
0.005	50	70
0.016	25	35
0.100	7.5	15

TABLE 2 Effect of electrolyte shielding on the total image energy at selected points along the axis of a gap junction analogue as a function of ionic strength (W = 150 Å, a_0 = 8.0 Å); energies are in kJ mol^{-1}

z/Å I/M	0.000	0.005	0.016	0.1
00.0	10.4	3.0	1.9	0.6
15.0	10.2	3.0	1.9	0.6
30.0	9.4	3.0	1.9	0.6
45.0	7.9	2.9	1.9	0.6
60.0	5.3	2.6	1.7	0.55
67.5	3.4	2.0	1.4	0.5
75.0	1.3	0.8	0.6	0.2
82.5	0.45	0.3	0.2	0.0
90.0	0.2	0.1	0.05	0.0

TABLE 4 Effect of electrolyte shielding on the total image energy at selected points along the axis of a porin analogue as a function of ionic strength (W = 55 Å, a_0 = 6.0 Å); energies are in kJ mol^{-1}

z/Å I/M	0.000	0.005	0.016	0.1
00.0	8.9	3.9	2.8	1.2
10.0	8.0	3.7	2.7	1.2
20.0	5.0	3.1	2.3	1.1
22.5	3.9	2.6	2.0	0.9
25.0	2.8	2.0	1.5	0.7
27.5	1.6	1.2	0.9	0.4
30.0	1.0	0.7	0.55	0.2
32.5	0.6	0.4	0.3	0.1
35.0	0.4	0.3	0.2	0.05

TABLE 5 Effect of ionic strength on axial separation at which the image interactions between a pair of ions in the porin analogue channel are below 10 mV and 20 mV, respectively

I/M	Image interaction < 20 mV z/Å	Image interaction < 10 mV z/Å
0.000	42.5	50
0.005	35	45
0.016	27.5	37.5
0.100	10	17.5

The qualitative features are the same for porins, assuming as geometrical parameters, $W = 55$ Å, $a_0 \approx 6$ Å (Garavito et al., 1983; for review see Benz, 1987). The major results are summarized in Tables 4 and 5. Because the channel is of smaller diameter, less electrolyte can enter and shielding is not as dramatic. Nonetheless, the peak of the image potential is only 0.5 kT at 0.1 M, 13% of its value in electrolyte free solution. Again, electrolyte shielding essentially neutralizes the influence of the surrounding low dielectric domain and most of the energy increase takes place in the channel entrance (the first 5–7.5 Å). The results presented in Table 4 are somewhat surprising in light of experimental results (Benz et al., 1980; Roos et al., 1982). They found no noticeable effect of concentration on the conductance of porin channels from either *Salmonella typhimurium* or rat liver mitochondria; we would expect a measurable reduction of ~50% for a concentration change from 0.1 to 0.01 M. There are a number of possible reasons for this difference. The porins, over most of their length, might have radii substantially >6 Å; the image barriers could then be considerably reduced. Alternatively, at the higher ionic strength, the focussing effect of the low dielectric constant domain is not as significant; the ions would be able to diffuse away from the axis more readily. Consequently the diffusional path length would increase and the conductance would be reduced. At low concentrations, the ions would be more likely to diffuse along the axial path.

Multiple occupancy is again readily accomplished at physiological electrolyte concentrations. The 20 mV total interaction level is reached for ions separated by 17.5 Å (at 0.1 M); similar reduction is only attained if the ions are >35 Å apart (at 0.005 M). If there were no electrolyte present, multiple occupancy would be highly unlikely.

We would like to thank Rod McKinnon for helpful discussions and a critical reading of the manuscript.

This work was supported by grant GM-28643 from the National Institutes of Health, instrumentation grants from the National Institutes of Health and National Science Foundation (at Brandeis University), and by grants from the National Institutes of Health, National Science Foundation, and the Robert A. Welch Foundation (at the University of Houston). J. A. McCammon is the recipient of the G. H. Hitchings Award from the Burroughs Wellcome Fund.

Received for publication 26 September 1988 and in final form 23 January 1989.

REFERENCES

Benz, R., J. Ishii, and T. Nakae. 1980. Determination of ion permeability through the channels made of porins from the outer membrane of *Salmonella typhimurium* in lipid bilayer membranes. *J. Membr. Biol.* 56:19–29.

Benz, R. 1987. Porin from bacterial and mitochondrial outer membranes. *Crit. Rev. Biochem.* 19:145–190.

Dani, J. A. 1986. Ion-channel entrances influence permeation. Net charge, size, shape, and binding considerations. *Biophys. J.* 49:607–618.

Flagg-Newton, J., I. Simpson, and W. R. Loewenstein. 1979. Permeability of the cell-to-cell membrane channels in mammalian cell junction. *Science (Wash. DC).* 204:404–407.

Garavito, R. M., J. Jenckins, J. N. Jansonius, R. Karlsson, and J. P. Rosenbusch. 1983. X-ray diffraction analysis of matrix porin, an integral membrane protein from *Escherichia Coli* outer membrane. *J. Mol. Biol.* 164:313–327.

Jordan, P. C. 1981. Energy barriers for the passage of ions through channels. Exact solution of two electrostatic problems. *Biophys. Chem.* 13:203–212.

Jordan, P. C. 1982. Electrostatic modeling of ion pores. Energy barriers and electric field profiles. *Biophys. J.* 39:157–164.

Jordan, P. C. 1984*a*. The total electrostatic potential in a gramicidin channel. *J. Membr. Biol.* 78:91–102.

Jordan, P. C. 1984*b*. Effect of pore structure on energy barriers and applied voltage profiles. I. Symmetrical channels. *Biophys. J.* 45:1091–1100.

Jordan, P. C. 1986. Ion channel electrostatics and the shape of channel proteins. *In* Ion Channel Reconstitution. C. Miller, editor. Plenum Publishing Corp., New York. 37–55.

Jordan, P. C., R. J. Bacquet, and J. A. McCammon. 1988. The influence of electrolyte shielding on the permeability of transmembrane ion channels. *Biophys. J.* 53:514a. (Abstr.)

Klapper, I., R. Hagstrom, R. Fine, K. Sharp, and B. Honig. 1986. Focusing of electric fields in the active site of Cu-Zn superoxide dismutase: effects of ionic strength and amino-acid modification. *Proteins Struc. Func. Gen.* 1:47–59.

Levitt, D. G. 1978. Electrostatic calculations for an ion channel. I. Energy and potential profiles and interactions between ions. *Biophys. J.* 22:209–219.

Levitt, D. G. 1985. Strong electrolyte continuum theory solution for equilibrium profiles, diffusion limitation, and conductance in charged ion channels. *Biophys. J.* 48:19–31.

Levitt, D. G. 1986. Interpretation of biological ion channel flux data. Reaction-rate versus continuum theory. *Annu. Rev. Biophys. Chem.* 15:29–57.

Levitt, D. G., and E. R. Decker, 1988. Electrostatic radius of the gramicidin channel determined from voltage dependence of H^+ ion conductance. *Biophys. J.* 53:33–38.

Makowski, L., D. L. D. Caspar, W. C. Phillips, and D. A. Goodenough, 1984. Gap junction structures. V. Structural chemistry inferred from x-ray diffraction measurements on sucrose accessibility and trypsin susceptibility. *J. Mol. Biol.* 174:449–481.

Peskoff, A., and D. M. Bers, 1988. Electrodiffusion of ions approaching the mouth of a conducting membrane channel. *Biophys. J.* 53:863–875.

Roos, N., R. Benz, and D. Brdiczka. 1982. Identification and characterization of the pore-forming protein in the outer membrane of rat liver mitochondria. *Biochim. Biophys. Acta.* 686:204–215.

Scarborough, J. B. 1962. Numberical Mathematical Analysis. Oxford Press, London.

Unwin, P. N. T., and G. Zampighi, 1980. Structure of the junction between communicating cells. *Nature (Lond.)*. 283:545–549.

Warwicker, J., and J. C. Watson, 1982. Calculations of electric potential in the active site cleft due to α-helix dipoles. *J. Mol. Biol.* 157:671–679.

Schwartzman, G., H. Weigandt, B. Rose, A. Zimmerman, D. Ben-Haim, and W. R. Loewenstein. 1982. Diameter of cell-to-cell junctional membrane channels as probed with neutral molecules. *Science (Wash. DC)*. 213:551–553.

Vayl, I. S., and P. C. Jordan, 1987. Electrostatic modeling of ion pores. Multipolar sources. *Biophys. Chem.* 27:7–13.